An Interhemispheric Tropical Sea Level Seesaw due to El Niño Taimasa

MATTHEW J. WIDLANSKY

International Pacific Research Center, University of Hawai'i at Mānoa, Honolulu, Hawaii

AXEL TIMMERMANN

International Pacific Research Center, and Department of Oceanography, University of Hawai'i at Mānoa, Honolulu, Hawaii

SHAYNE MCGREGOR

Climate Change Research Centre, and ARC Centre of Excellence for Climate System Science, University of New South Wales, Sydney, New South Wales, Australia

MALTE F. STUECKER

Department of Meteorology, University of Hawai'i at Mānoa, Honolulu, Hawaii

WENJU CAI

CSIRO Marine and Atmospheric Research, Aspendale, Australia

(Manuscript received 17 May 2013, in final form 23 September 2013)

ABSTRACT

During strong El Niño events, sea level drops around some tropical western Pacific islands by up to 20–30 cm. Such events (referred to as *taimasa* in Samoa) expose shallow reefs, thereby causing severe damage to associated coral ecosystems and contributing to the formation of microatolls. During the termination of strong El Niño events, a southward movement of weak trade winds and the development of an anomalous anticyclone in the Philippine Sea are shown to force an interhemispheric sea level seesaw in the tropical Pacific that enhances and prolongs extreme low sea levels in the southwestern Pacific. Spectral features, in addition to wind-forced linear shallow water ocean model experiments, identify a nonlinear interaction between El Niño and the annual cycle as the main cause of these sea level anomalies.

1. Introduction

Recurring below-normal sea levels in the tropical western Pacific are a well-known aspect of the El Niño–Southern Oscillation (ENSO) with sometimes damaging consequences for coastal ecosystems and vulnerable island communities. Interannual variability of sea levels is largely caused by a pronounced ''zonal seesaw'' of the tropical Pacific thermocline depth associated with ENSO (e.g., Jin 1997; Wyrtki 1984). During El Niño, weak equatorial trade winds cause the thermocline to rise in the tropical western Pacific and deepen to the east, while the overlying sea surface height generally mirrors these subsurface changes (Delcroix 1998). These western Pacific surface anomalies typically reach values of up to 10 cm (Merrifield et al. 1999), although sea level drops of 30 cm have been observed during strong El Niño events (Becker et al. 2012). The opposite sea level pattern occurs during La Niña, but anomalies rarely exceed 10 cm above the mean in the western Pacific.

Sometimes though, a meridional gradient in thermocline depth (and sea level) also develops in response to ENSO in the western Pacific (Alory and Delcroix 2002; Becker et al. 2012; Chowdhury et al. 2006; Delcroix 1998; Nidheesh et al. 2013). Meridional asymmetry in sea level is most pronounced during strong El Niño events, such as occurred in 1997/98 (Alory and Delcroix 2002) when the South Pacific convergence zone [SPCZ; the largest rainfall band in the Southern Hemisphere;

Corresponding author address: M. J. Widlansky, International Pacific Research Center, University of Hawai'i at Mānoa, 1680 East–West Rd., Honolulu, HI 96822.
E-mail: mwidlans@hawaii.edu

DOI: 10.1175/JCLI-D-13-00276.1

© 2014 American Meteorological Society

Unauthenticated | Downloaded 04/28/25 08:15 PM UTC

Vincent (1994); Widlansky et al. (2011)] collapsed almost completely onto the equator (Cai et al. 2012; Vincent et al. 2011). After a strong El Niño, below-normal sea levels persist in the southwestern Pacific long after sea surface heights have returned to normal in the northern Pacific. This ''meridional seesaw'' pattern of the thermocline (e.g., Alory and Delcroix 2002) is characterized by enhanced spectral energy on periods of 9 and 15 months (Wang et al. 1999), suggesting an influence of the annual cycle on sea level variability in the western Pacific.

One consequence of prolonged sea level drops of large magnitude is the repeated exposure of shallow reefs to air at low tide. This exposure causes the top portions of coral heads to die off (Pirhalla et al. 2011), often creating what are known as microatolls (Woodroffe et al. 2003) on shallow reef flats that are found in wide areas of the western Pacific coastal reef ecosystem (Cheng and Gaskin 2011). Samoans refer to coral die-offs caused by such low sea level events as *taimasa* [pronounced (kai' ma'sa); translation from Samoan to English is ''foul smelling tide'']; a term highlighted recently by Pirhalla et al. (2011) and related to the odor emanating from decaying coral. Very low sea levels, or taimasa, affect South Pacific islands mostly during strong El Niño events (Table 1: 1982/83 and 1997/98, in addition to 1991/92, saw much below-normal sea levels). The effects of added stress to reef ecosystems brought on by low sea level can be wide ranging, causing not only coral mortality but also decreased biological productivity on nearshore reef flats that strongly impacts island societies (Kilarski and Everson 2008). Yet in spite of the potential high ecological and societal impacts of taimasa in the tropical southwestern Pacific, much uncertainty remains about why low sea levels sometimes persist in the Southern Hemisphere and whether this persistence is predictable seasons ahead.

Here, we set out to explain the hemispheric asymmetry in the ENSO–sea level response by providing a physical framework to combine the zonal seesaw mechanism, which modifies the tropical thermocline on interannual time scales, with the higher-frequency meridional seesaw of the sea level. Data and the methodology used to study the surface wind response to ENSO and its forcing on sea level anomalies are presented in section 2. In section 3, we quantify and describe the hemispheric difference in the western Pacific sea level response to strong El Niño patterns. The role of the annual cycle of wind stress anomalies on sea level is then discussed in section 4. Finally, a summary of results is provided in section 5 along with ideas for achieving enhanced predictability of future sea level anomalies.

2. Surface wind pattern associated with ENSO

To study the western Pacific climate and sea level response to ENSO, monthly mean observations (including reanalysis products) of the lower atmosphere and near-surface ocean are utilized for the period 1979–2011. The observations consist of surface wind stress data from the Interim European Centre for Medium-Range Weather Forecasts (ECMWF) Re-Analysis (ERA-Interim; Dee and Uppala 2009); rainfall from the Global Precipitation Climatology Project (GPCP) merged monthly precipitation dataset, version 2 (Adler et al. 2003); and sea surface height and ocean currents from the ECMWF operational Ocean Reanalysis (ORA) system 4 (Mogensen et al. 2012). For all variables, anomalies are computed relative to a mean seasonal cycle based on the respective 33-yr climatology, except for rainfall, which does not have data available for all of 2011; a 32-yr climatology is used instead. Variability on interannual time scales is highlighted, as opposed to either multidecadal time scales (Merrifield et al. 2012) or the longer-term sea level rise attributed to greenhouse warming (Merrifield and Maltrud 2011), by removing any linear trend from the data prior to linearly regressing each field onto the two leading modes of wind stress variability.

Figure 1a shows the first and second principal components (PC1 and PC2) of the empirical orthogonal function (EOF) decomposition of the equatorial (10°S–10°N, 100°E–60°W) wind stress anomaly field, computed as in McGregor et al. (2012b) and Stuecker et al. (2013) to isolate interannual wind changes in the equatorial Pacific. We highlight the three highest peaks of the PC1 time series and classify these periods as strong El Niño events (1982/83, 1997/98, as well as the more moderate 1991/92 event) that match the extreme zonal SPCZ events classified in Cai et al. (2012) and the lowest sea level anomalies in the tropical southwestern Pacific (Table 1). During the two strongest El Niño events (i.e., 1982/83 and 1997/98), PC2 abruptly switches from negative to positive and peaks shortly after PC1, which is also positive. The PC2 sign change during 1991/92 is less abrupt and this event will be compared, in section 3, with the two stronger events to illustrate how the second EOF mode of wind stress variability affects the western Pacific sea level response to El Niño. These results are robust to reasonable changes in the domain of the EOF analysis (e.g., similar PCs were calculated using wind stress anomalies that were extended into the tropics or confined to the western half of the Pacific: 20°S–20°N or 120°E–150°W).

Associated linear regressions of wind stress, wind stress curl, sea surface height, and near-surface current anomalies onto PC1 and PC2 are shown for the tropical

Unauthenticated | Downloaded 04/28/25 08:15 PM UTC

TABLE 1. Yearly climate and sea level characteristics in the tropical southwestern Pacific (taimasa events are set in boldface). ENSO classification, zonal SPCZ occurrence, minimum sea level anomaly in the southwest Pacific (15.5°S–1.5°N, 150.5°E–165.5°W), tropical cyclone (TC) genesis count, and rainfall anomaly are calculated for the Southern Hemisphere TC season (July year n to June year $n + 1$). TC genesis counts and rainfall anomalies are calculated for the four regions of greatest interannual variability as defined in Vincent et al. (2011): Tahiti, 5°–20°S, 165°–130°W; Tuvalu, 5°–13°S, 165°E–165°W; Fiji, 13°–25°S, 165°E–165°W; and Coral Sea, 10°–20°S, 143°–165°E.

				TC genesis[d] count and rainfall[e,f] anomaly (%)							
TC season	ENSO category[a]	Zonal SPCZ?[b]	Sea level[c] anomaly southwest Pacific (cm)	Tahiti		Tuvalu		Fiji		Coral Sea	
1979/80	Neutral	No	−3.2	0	(96)	4	(97)	1	(93)[f]	4	(90)
1980/81	Neutral	No	−2.6	3	(101)	4	(94)	4	(92)[f]	1	(91)
1981/82	Neutral	No	−0.6	0	(77)	2	(92)	0	(99)	0	(108)
1982/83	**El Niño**	**Yes**	**−19.5**	**6**	**(139)[f]**	**4**	**(123)[f]**	**2**	**(101)**	**1**	**(88)**
1983/84	La Niña	No	−17.9	0	(102)	2	(92)	1	(98)	9	(112)
1984/85	La Niña	No	−5.7	1	(108)	2	(97)	0	(102)	6	(115)
1985/86	Neutral	No	1.1	1	(92)	1	(89)	2	(96)	4	(112)
1986/87	El Niño	No	−7.9	1	(101)	7	(119)	2	(101)	3	(75)[f]
1987/88	El Niño	No	−9.0	1	(113)	2	(115)	2	(108)[f]	1	(84)
1988/89	La Niña	No	−2.9	1	(75)[f]	1	(84)	5	(104)	4	(132)[f]
1989/90	Neutral	No	−1.8	1	(95)	2	(93)	1	(95)	1	(100)
1990/91	Neutral	No	1.7	0	(77)	2	(90)	0	(93)[f]	1	(107)
1991/92	**El Niño**	**Yes**	**−15.6**	**3**	**(125)[f]**	**6**	**(112)**	**1**	**(98)**	**0**	**(83)**
1992/93	Neutral	No	−7.5	1	(113)	4	(111)	1	(100)	2	(77)[f]
1993/94	Neutral	No	−5.2	0	(92)	1	(106)	1	(100)	1	(87)
1994/95	El Niño	No	−4.2	0	(109)	1	(112)	0	(101)	1	(78)[f]
1995/96	La Niña	No	−1.9	0	(99)	1	(88)	2	(95)	2	(101)
1996/97	Neutral	No	−1.2	1	(95)	6	(106)	2	(105)	2	(107)
1997/98	**El Niño**	**Yes**	**−17.1**	**5**	**(181)[f]**	**6**	**(130)[f]**	**2**	**(104)**	**1**	**(84)**
1998/99	La Niña	No	−13.0	1	(89)	0	(92)	1	(103)	6	(126)[f]
1999/00	La Niña	No	−0.7	1	(75)[f]	0	(71)[f]	5	(94)	3	(126)[f]
2000/01	La Niña	No	0.2	2	(88)	1	(84)[f]	1	(101)	2	(109)
2001/02	Neutral	No	1.3	1	(88)	2	(98)	0	(99)	2	(91)
2002/03	El Niño	No	0.0	1	(107)	3	(121)[f]	4	(109)[f]	0	(86)
2003/04	Neutral	No	2.0	0	(106)	0	(102)	2	(99)	3	(92)
2004/05	El Niño	No	−0.1	1	(119)	4	(107)	2	(105)	0	(88)
2005/06	La Niña	No	3.1	0	(89)	1	(91)	3	(98)	3	(108)
2006/07	El Niño	No	0.7	0	(90)	4	(107)	1	(100)	2	(97)
2007/08	La Niña	No	4.0	0	(75)[f]	2	(86)	1	(110)[f]	2	(120)
2008/09	La Niña	No	2.7	2	(78)	1	(77)[f]	2	(94)	3	(120)
2009/10	El Niño	No	−6.1	0	(106)	5	(112)	2	(105)	2	(104)
2010/11	La Niña	No	0.9	0		0		6		3	
		TC genesis climatology		1		3		2		2	

[a] Niño-3.4 index in formation available online (http://www.cpc.ncep.noaa.gov/products/analysis_monitoring/ensostuff/ensoyears.shtml).
[b] See Cai et al. (2012) and Vincent et al. (2011) for details.
[c] ORA sea surface height (Mogensen et al. 2012).
[d] Southwest Pacific Enhanced Archive for Tropical Cyclones (SPEArTC; http://apdrc.soest.hawaii.edu/projects/speartc/).
[e] GPCP rainfall (Adler et al. 2003).
[f] Rainfall anomalies (% of climatology) in the wettest 90th percentile and driest 10th percentile for each region.

western and central Pacific in Figs. 1b–e (regression coefficients). As seen from the regression of the wind stress onto PC1 (Fig. 1b, positive phase of PC1), the first EOF is the equatorially quasi-symmetric wind stress pattern associated with ENSO, as characterized by westerly wind anomalies in the equatorial western Pacific during El Niño (Stuecker et al. 2013). PC2 (Fig. 1c) represents the termination phase of strong El Niño events when an anomalous western North Pacific anticyclone develops (i.e., the Philippine Sea anticyclone) (e.g., Wang et al. 1999), along with a southward-shifted westerly wind anomaly east of the date line (Harrison and Vecchi 1999; McGregor et al. 2012b; Vecchi and Harrison 2003, 2006). Meridional shear in the South Pacific adjacent to the southward-shifted westerly wind anomaly causes a cyclonic wind stress curl (centered near 10°S, 165°W) and hence oceanic Ekman suction. Increased rainfall is also observed in the central equatorial Pacific when PC2 is positive (Fig. 2b), while drying occurs to the west and south, indicating a shift in location

Unauthenticated | Downloaded 04/28/25 08:15 PM UTC

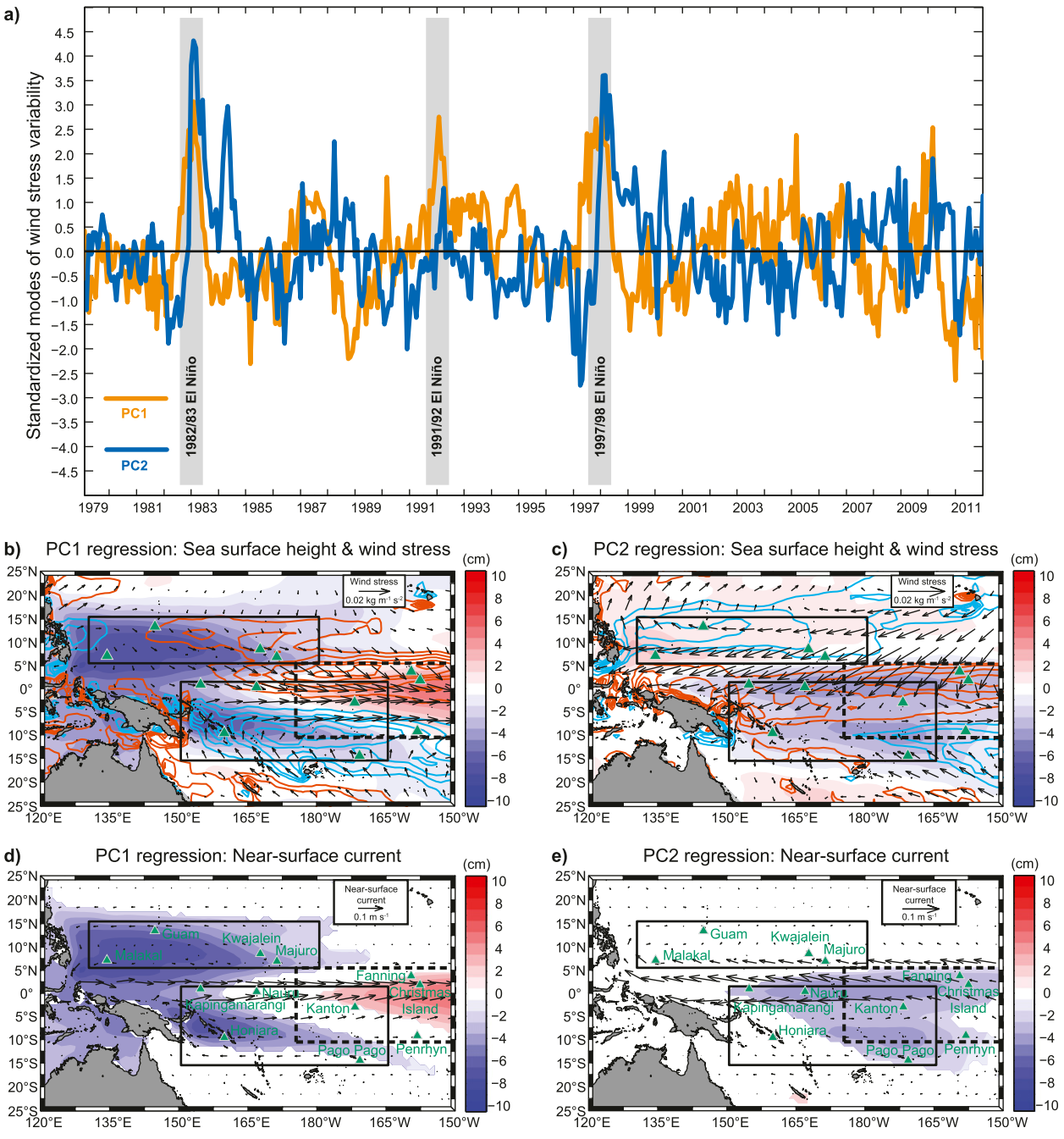

FIG. 1. Two principal modes of wind stress variability in the tropical Pacific and their associated linear regressions of sea surface height and wind stress. (a) PC1 (orange) and PC2 (blue) explain 26.3% and 14.9%, respectively, of the equatorial wind stress variance. Gray bars indicate three strong El Niño events referred to throughout the text. (b),(c) Regressions of sea surface height (cm, color shading), wind stress ($\mathrm{Kg\,m^{-1}\,s^{-2}}$, vectors), and wind stress curl (contours starting at $\pm 0.5 \times 10^{-8}\,\mathrm{Kg\,m^{-2}\,s^{-2}}$) onto PC1 and PC2, respectively. Orange (blue) contours depict positive (negative) wind stress curl anomalies. (d),(e) Ocean current regressions ($\mathrm{m\,s^{-1}}$, vectors) from ORA averaged over the top six levels (5–56 m) to best describe the near-surface zonal and meridional flow. Color shading indicates statistically significant ($p > 95\%$) sea surface height regressions [as in (b),(c)] according to a two-sided t test of correlation coefficients from the respective regressions. The effective number of independent samples at each grid ($N_{\mathrm{eff}} = 38$, domain average) is calculated as half the number of e-folding times of the sea surface height autocorrelation (Leith 1973). Black boxes represent the northwest Pacific (5.5°–15.5°N, 130.5°E–179.5°W), southwest Pacific (15.5°S–1.5°N, 150.5°E–165.5°W), and central Pacific (10.5°S–5.5°N, 175.5°E–149.5°W; dashed) averaging regions. Enclosed triangles indicate tide gauge stations used in this study.

Unauthenticated | Downloaded 04/28/25 08:15 PM UTC

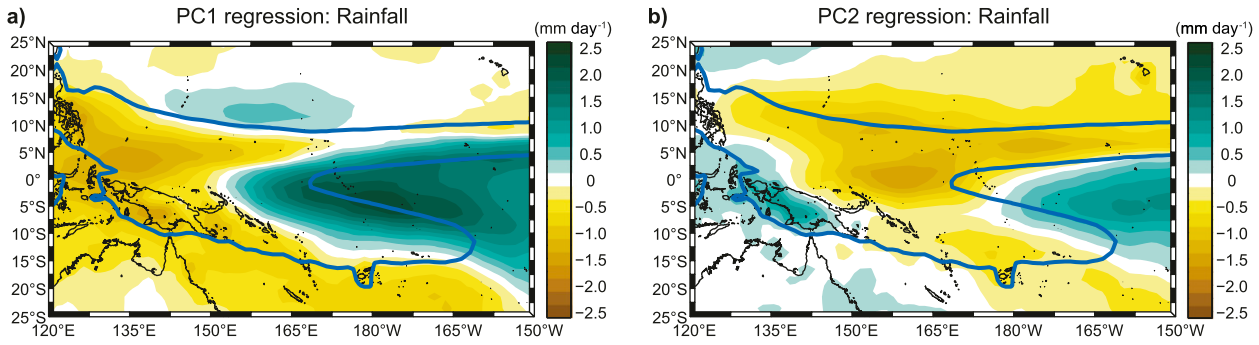

FIG. 2. Linear regressions of rainfall (mm day^{-1}, color shaded) onto (a) PC1 and (b) PC2. Pacific rainbands (e.g., Widlansky et al. 2013) are enclosed by the 5 mm day^{-1} annual climatology.

of the SPCZ farther toward the equator compared to when only PC1 is positive (Fig. 2a). During such zonal SPCZ events, Tahiti experiences significantly above normal rainfall and a higher frequency of tropical cyclone genesis, while regions to the southwest, such as the Coral Sea, experience drying and reduced occurrence of tropical cyclones (Cai et al. 2012; Vincent et al. 2011) (see also Table 1).

Regression of sea surface height onto PC1 (Fig. 1b, shading; Fig. 1d, shading regressions significant at the 95% level) shows the canonical sea level response to El Niño. At the peak of El Niño (PC1 $>$ 0), sea levels are lower in the western Pacific and higher in the central and eastern equatorial Pacific (i.e., the zonal seesaw pattern). Near-surface current anomalies are westerly (Fig. 1d), indicating a strengthening of the Equatorial Counter Current and drainage of the West Pacific Warm Pool (Wyrtki 1989). The respective regression onto PC2 (Fig. 1c) shows, on the other hand, the meridional seesaw sea surface height response caused by establishment of the Philippine anticyclone (thermocline deepens in the northwestern Pacific and sea levels rise) along with southward movement of the westerly wind anomaly and the associated cyclonic wind stress curl (statistically significant sea level drop in the southwestern Pacific; Fig. 1e). Shortly after the peak of strong El Niño events (PC2 $>$ 0), equatorial current anomalies associated with this mode reverse (Fig. 1e) and sea levels return to near normal in most of the northwestern Pacific; however, sea levels remain depressed for some time south of 5°N [i.e., the meridional seesaw described in detail by Alory and Delcroix (2002)].

Near the end of strong El Niño events, the SPCZ collapses almost completely onto the equator (Cai et al. 2012). To the south of the increased rainfall (Fig. 2b), cyclonic wind stress curl anomalies (negative anomalies in the South Pacific; blue contours in Fig. 1c) force oceanic Ekman suction (Timmermann et al. 2010), which causes a shoaling of the thermocline and a drop of sea level in much of the tropical southwestern Pacific (McGregor et al. 2012a) long after the northwestern Pacific has returned to normal. We hypothesize that the persistence of negative sea level anomalies south of the equator is driven in part by an ENSO-modulated annual cycle of the winds (Stuecker et al. 2013) and the associated cyclonic wind stress curl that drives local Ekman pumping anomalies and Rossby waves, causing the thermocline to remain shallower than normal in the southwestern Pacific until well after the termination of El Niño.

3. Asymmetric western Pacific sea level response during strong El Niño events

The meridional difference in sea level anomalies is captured by defining two regions in the western Pacific; a northwest and southwest box, as depicted in Fig. 1. Within these boxes, we chose nine tide gauge stations (indicated in Fig. 1 and listed in Table 2) from the University of Hawaii Sea Level Center Research Quality and Fast Delivery databases (UHSLC; e.g., Merrifield et al. 1999). These stations are chosen based on their location within either the northwest Pacific (four stations) or southwest Pacific (five) and for having long records, matching closely the satellite era (1979–2011) of wind stress and sea surface height reanalysis products. Three additional stations characterize the central Pacific region (enclosed by only the dashed box in Fig. 1). Tide gauge anomalies are computed relative to a mean seasonal cycle based on the 33-yr climatology of each station and the linear trend is removed, following the procedure used for sea surface height obtained from the ORA products. The time series of every tide gauge in the northwest and southwest Pacific is shown in Fig. 3, along with the multistation mean for the respective regions (thick lines).

Unauthenticated | Downloaded 04/28/25 08:15 PM UTC

TABLE 2. Tide gauge stations from the UHSLC. Short data gaps during 1979–2011 are left blank in the individual station time series (Figs. 3 and 4d).

Station name	Region	Location
Guam	Northwest Pacific	13.6°N, 144.9°E
Kwajalein	Northwest Pacific	8.7°N, 167.7°E
Majuro	Northwest Pacific	7.1°N, 171.4°E
Malakal	Northwest Pacific	7.3°N, 134.5°E
Honiara	Southwest Pacific	9.4°S, 160.0°E
Kanton	Southwest Pacific	2.8°S, 171.7°W
Kapingamarangi	Southwest Pacific	1.1°N, 154.8°E
Nauru	Southwest Pacific	0.5°N, 166.9°E
Pago Pago	Southwest Pacific	14.3°S, 170.7°E
Christmas Island	Central Pacific	2.0°N, 157.5°W
Fanning	Central Pacific	3.9°N, 159.4°W
Penrhyn	Central Pacific	9.0°S, 158.1°W

Apparent from Fig. 3 is the close correspondence between individual station time series and their respective multistation averages. Station agreement is especially strong in the northwest Pacific during the 1982/83, 1991/92, and 1997/98 El Niño events (highlighted) and shortly after each event peak in the southwest Pacific. All tide gauge stations recorded below-normal sea levels during these respective times. In the northwest Pacific, sea level dropped to 15–30 cm below normal by the peak of El Niño, before abruptly returning to near-normal or slightly above-normal heights. The magnitude of the sea level anomalies in the southwest Pacific (see also Table 1, which retains the linear trend) is similar to the northwest Pacific; however, as a result of the effects of wind EOF2 on the thermocline depth–sea surface height, the southern tide gauges record below-normal sea level for much longer. Averaging over the 33-yr period, the southwest Pacific tide gauge time series lags the northwest Pacific by 6 months with a peak correlation coefficient of 0.60 (Fig. 3, insert), but most of the lag is clearly attributable to the periods immediately after the two strongest El Niño events (1982/83 and 1997/98).

Tide gauge time series (Fig. 3) show a pronounced meridional asymmetry in the western Pacific sea level response to strong El Niño events. To quantify this meridional asymmetry, we calculate the difference between standardized sea level in the northwest and southwest Pacific regions (NWPAC minus SWPAC) using tide gauge station data and also ORA sea surface height anomalies to best cover the spatial domains. The NWPAC minus SWPAC index is somewhat smoother for the ORA data (Fig. 4a), as averaging is performed over the black box regions as defined in Fig. 1 instead of individual stations (Fig. 4c). Regardless of dataset or

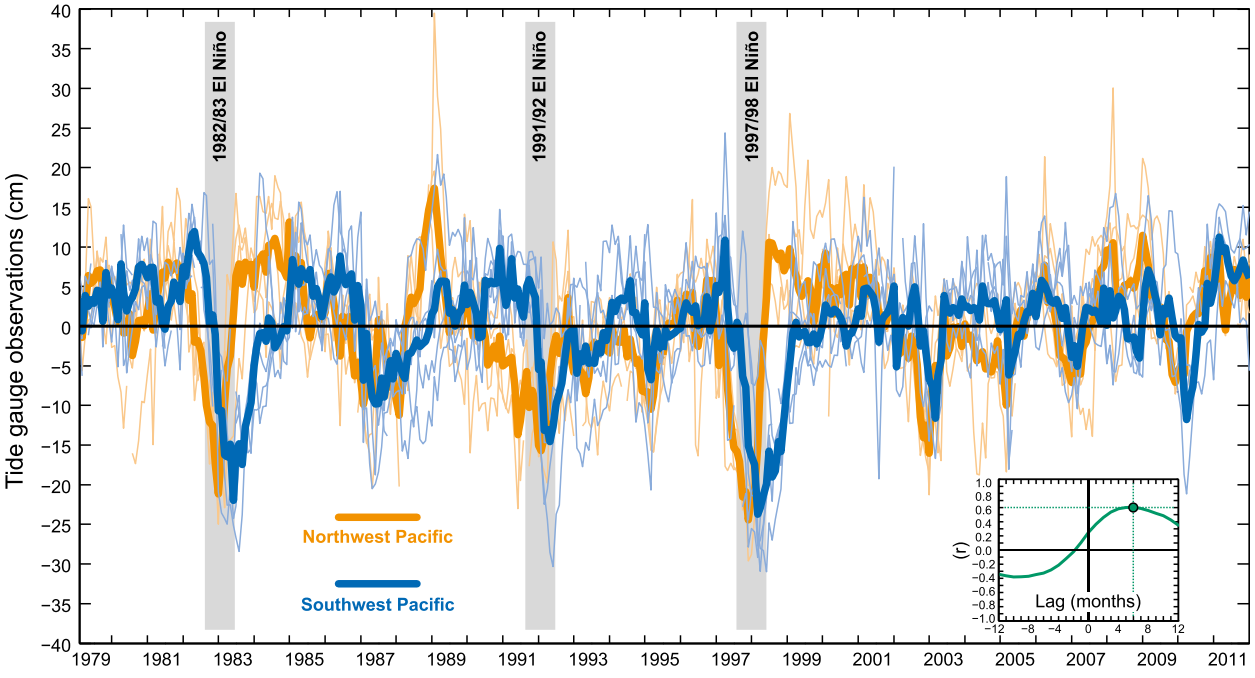

FIG. 3. Tide gauge observations in the northwest Pacific (orange) and southwest Pacific (blue) with the linear trend in each region removed. Thin lines represent individual tide gauge stations and thick lines represent the multistation averages. The green insert shows the correlation coefficient (r) between regions as a function of lag in months (southwest Pacific lags northwest Pacific). Correlations exceeding ±0.38 are statistically significant at the 95% confidence level according to a two-sided t test ($N_{\text{eff}} = 28$, based on the autocorrelation decay time scale of the southwest Pacific multistation average).

Unauthenticated | Downloaded 04/28/25 08:15 PM UTC

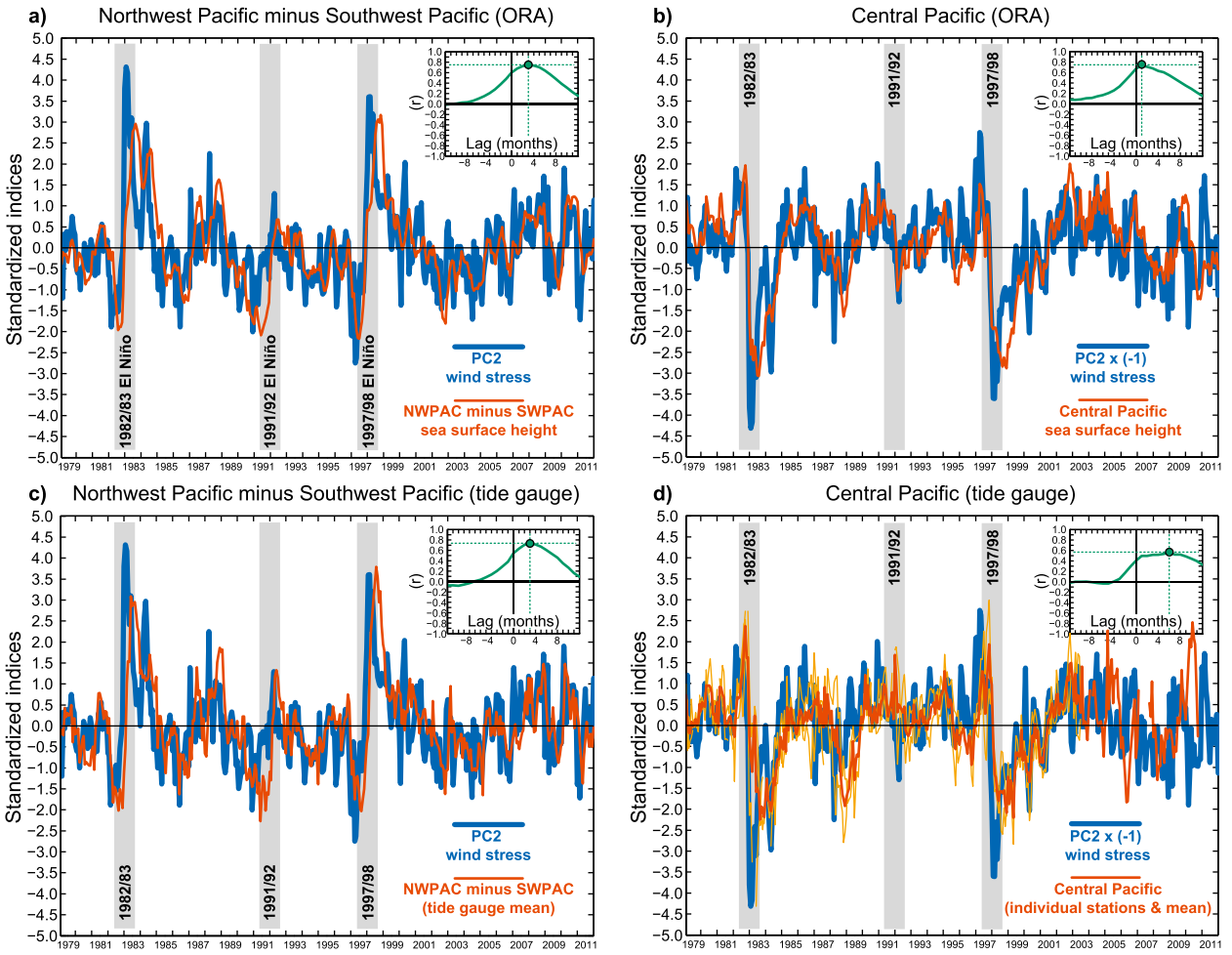

FIG. 4. Standardized indices of PC2 wind stress variability (blue) and sea level indices (orange). Green inserts show the correlation coefficient between PC2 and sea level as a function of lag in months (sea level lags PC2). (a) NWPAC minus SWPAC sea levels using ORA sea surface height. (b) As in (a), but showing PC2 × (−1) and the central Pacific sea level index. (c),(d) As in (a),(b), but with tide gauge data used instead of ORA sea surface height. Thick orange lines represent the average of all available stations. Thin orange lines in (d) indicate the limited number and completeness of the central Pacific tide gauge data (stations listed in Table 2). Critical values ($p > 95\%$) for the correlation coefficients are (a) 0.40, (b) 0.42, (c) 0.34, and (d) 0.38 based on respective autocorrelation decay time scales.

averaging technique, both standardized indices show peak hemispheric differences in sea level (exceeding 2.5 standard deviations above the mean) near the end of the 1982/83 and 1997/98 El Niño events, whereas the opposite phase of the meridional sea level seesaw (PC2 < 0; negative gradient) occurs in the onset phase of both events. For the 1991/92 event, in comparison, the NWPAC minus SWPAC index peak is much smaller because sea levels in the northwest Pacific did not recover as abruptly; hence, the gradient peak is not discernible from other periods of El Niño conditions. Clearly, the interhemispheric asymmetry in sea level is greatest during the two strongest El Niño events (1982/83 and 1997/98), which occurs simultaneously with the two largest peaks of wind stress PC2 (Fig. 1a; also underlain in Fig. 4). Interestingly, sea levels in the central Pacific are more than 2.5 standard deviations below normal during these two El Niño events (Figs. 4b and 4d, respectively, for ORA and tide gauge data) and these sea level drops are more abrupt than during any other time.

The NWPAC minus SWPAC index is closely related to PC2 of wind stress. For ORA sea surface height, the hemispheric gradient index lags PC2 by about 3 months with a peak correlation coefficient of 0.74 (Fig. 4a, insert). Central Pacific sea levels are also strongly anticorrelated with PC2 (Fig. 4b, insert), although sea surface heights east of the SPCZ drop more abruptly during PC2 peaks (highest correlation at 1 month lag, $r = 0.73$). These correlations are statistically significant

Unauthenticated | Downloaded 04/28/25 08:15 PM UTC

($p > 95\%$) and the 1–3-month lags are reasonable wind-forced oceanic adjustment time scales for the tropical Pacific sea level response to Ekman pumping associated with local wind stress forcing (see Qiu and Chen 2010, their Fig. 10). Similar correlations are found using the UHSLC tide gauge data (Figs. 4c,d, inserts), except for in the central Pacific after 2002 when only one station is available and there is a lack of agreement with ORA.

Comparing regressions of wind stress curl and sea surface height onto PC2 (Fig. 1c) discussed in section 2, we see that the southward movement of westerly wind anomalies and cyclonic curl is collocated with prolonged negative sea surface heights in the southwest Pacific, whereas sea surface heights return to normal north of 5°N. Those regressions, along with the strong correlation between PC2 of wind stress and the NWPAC minus SWPAC sea level index (Fig. 4a, insert), support our hypothesis that meridional asymmetry in the sea level response to ENSO is driven by time-varying surface wind anomalies and, in particular, the second EOF mode of tropical wind stress variability.

4. Role of the annual cycle

To further elucidate the influence of ENSO and the annual cycle on the interhemispheric sea level seesaw, we calculate the power spectra of the difference between the standardized NWPAC minus SWPAC sea level index (Fig. 5). We observe enhanced spectral energy on either side of the annual frequency ($1 - f_E$ or $1 + f_E$; i.e., between either 0.5–0.86 or 1.14–1.5 cycles yr^{-1}). These frequencies translate to periods of approximately 14–24 and 8–11 months, respectively, and are related to the combination tones between the annual cycle frequency ($f = 1$) and the dominant ENSO frequency band (f_E; 0.14–0.5 cycles yr^{-1} corresponding to a 2–7-yr-period band). Combination tones emerge through a nonlinear combination (for instance a product) of the underlying ENSO and annual cycle modes (Stuecker et al. 2013). It should be noted that, as a result of the specific representation of the atmospheric nonlinearity and ocean–atmosphere interaction, the $1 - f_E$ peak is more pronounced than its companion peak at $1 + f_E$. As shown by Stuecker et al. (2013), this combination mode appears in PC2 of the winds as a result of the nonlinear atmospheric response in the tropical western Pacific to combined annual cycle and ENSO forcing in sea surface temperature (SST). The high correlation between PC2 and the interhemispheric sea level gradient (Fig. 4a, insert) bears further witness to the role of combination mode dynamics in determining an important aspect of sea level variations in the tropical Pacific.

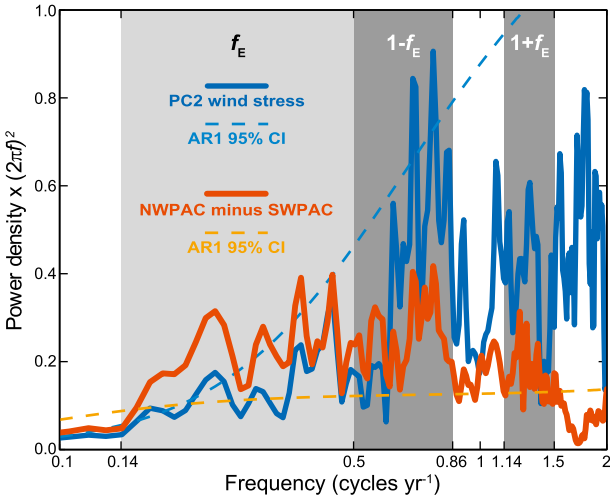

FIG. 5. Spectral power density calculated from the product of angular frequency squared and the power spectra of PC2 (blue) and the NWPAC minus SWPAC index (orange) obtained from the Multitaper Method (Thomson 1982) with three tapers. ENSO frequency (light gray box) is abbreviated f_E. Dark gray boxes indicate the near-annual combination tone frequency bands $1 - f_E$ and $1 + f_E$. The 95% confidence interval above the null hypothesis (autoregressive model of order one; AR1 obtained from the full frequency range) is indicated by dashed lines for the respective spectra (blue and orange).

To demonstrate the close physical linkage between wind PC2 and the interhemispheric sea level seesaw, and further support the statistical inferences (Fig. 1c), we conduct shallow water model (SWM) hindcast experiments forced with time-varying wind stress reconstructed from either PC1, PC2, or PC1 + PC2 of the observed wind stress shown in Fig. 1. The SWM used here is a 1.5-layer reduced-gravity linear model of the stratified tropical ocean with 1° horizontal resolution. Anomalous wind stresses drive motion in the top layer of the model, while the bottom layer is assumed motionless and infinitely deep [further details of the SWM are provided in McGregor et al. (2007, 2012a)]. To infer changes in sea level, we measure the vertical displacement of the thermocline, which in the SWM is the interface between the top and bottom model layers. Thermocline changes can be easily translated into sea level anomalies by using the reduced gravity of regressions between simulations and sea level data (see Timmermann et al. 2010). In the tropics, where thermocline depth changes are a good indicator of sea level anomalies, a 10-m reduction of the thermocline depth is approximately equivalent to a 5-cm drop in sea level (Rebert et al. 1985).

In response to prescribed PC1 and PC2 wind stress forcing, the regression patterns of the SWM experiments (i.e., the simulated thermocline depths regressed onto

Unauthenticated | Downloaded 04/28/25 08:15 PM UTC

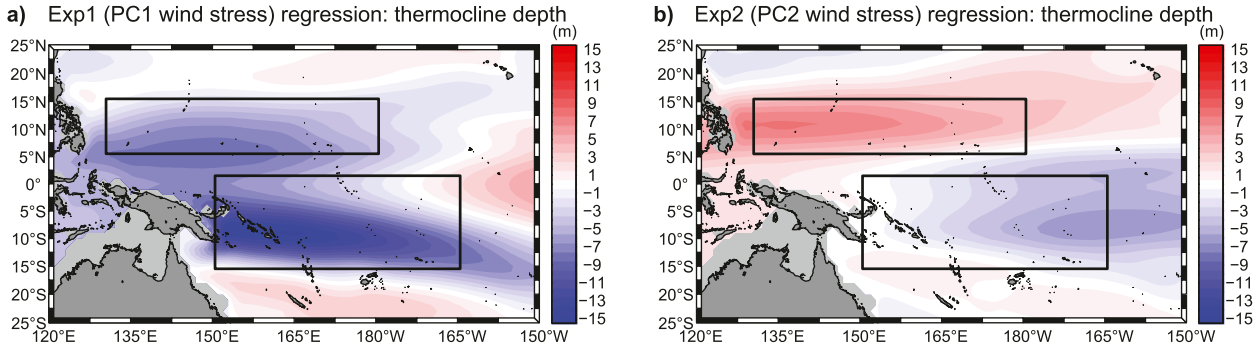

FIG. 6. Regressions of thermocline depth (m, color shading) from SWM experiments forced with anomalous wind stresses reconstructed from either (a) PC1 or (b) PC2 of the observations shown in Fig. 1. Black boxes represent the northwest Pacific and southwest Pacific averaging regions, as defined in Fig. 1.

either PC1 or PC2) are characterized by vertical displacements of the thermocline (Figs. 6a,b), which are in close spatial agreement with the observed sea surface height regressions (Figs. 1b,c) and of reasonable magnitudes. We note that the leading modes of the SWM simulations have time series highly correlated with the respective forcing time series (0.79 and 0.55); thus, to simplify the methods, we present maps of regression coefficients between the forcing time series and model output. During peaks in the PC1 wind stress, the simulated thermocline rises in the tropical western Pacific and deepens in the central equatorial Pacific (i.e., the SWM resolves the zonal seesaw response to ENSO) (see also Meinen and McPhaden 2000). These thermocline depth anomalies are associated with a lowering and rising of sea level in the western and central Pacific, respectively, as well as Kelvin and Rossby wave dynamics. The largest thermocline rise (sea level drop) is simulated in a diagonal band near the position of the observed SPCZ during El Niño, where the strongest cyclonic wind stress curl anomalies occur (Fig. 1b). In comparison, the experiment forced with PC2 wind stress (Fig. 6b) shows a deepening thermocline in the tropical northwestern Pacific (anticyclonic wind stress curl and higher sea levels) and a shallow thermocline to the south (cyclonic wind stress curl and below-normal sea levels). Note that the highest correlations would be expected for lags of about 3 months (Fig. 4a). Most importantly, the thermocline depth pattern in the SWM experiment forced only with PC2 wind stress (Fig. 6b) closely matches the meridional asymmetry observed in the sea surface height regression onto PC2 (Fig. 1c).

The shallow southwestern Pacific thermocline in the PC2 experiment supports the hypothesis that the southward westerly wind shift and the corresponding cyclonic wind stress curl, which is essentially produced by nonlinear interaction between the annual cycle and ENSO (Stuecker et al. 2013), are sufficient to prolong below-normal sea levels for the island groups affected by the SPCZ (listed in Table 1). Further, the SWM hindcast experiment forced with PC1 + PC2 more closely simulates the observed southwest Pacific sea level time series compared to either the PC1 or PC2 experiments (Fig. 7a). While the correlation coefficient between sea level observations and the PC1 experiment exceeds 0.5 (25% of variance explained) in most of the tropical Pacific (Fig. 7b), PC1 has essentially no predictive skill in a horizontal chevron-shaped dipole region centered around the date line in the equatorial Pacific (i.e., adjacent to the SPCZ and ITCZ) (see also Zhang and Church 2012, their Fig. 3). Adding PC2 wind stress enhances the correlation coefficient in this particular region (Fig. 7c)—thus, explaining the close temporal correlation noted in the southwest Pacific between the PC1 + PC2 hindcast experiment and observed sea level (Fig. 7a; $r = 0.86$)—and suggests a new metric for achieving increased predictability of future prolonged low sea level events.

5. Summary and opportunities for enhanced predictability

We have shown that certain El Niño events have severe combined sea level and climate effects on South Pacific islands. These effects include extremely low sea levels accompanied by exposed shallow reefs (*taimasa*), reduced rainfall in some areas, and increased tropical cyclone activity in others (Cai et al. 2012; Vincent et al. 2011) (see also Table 1). We shall refer to specific events that combine these threats as El Niño taimasa, alluding to their damaging effects on shallow reefs in Samoa and the nearby regions. The three observed El Niño taimasa events were those of 1982/83, 1991/92, and 1997/98, which are set apart from other strong El Niño events,

Unauthenticated | Downloaded 04/28/25 08:15 PM UTC

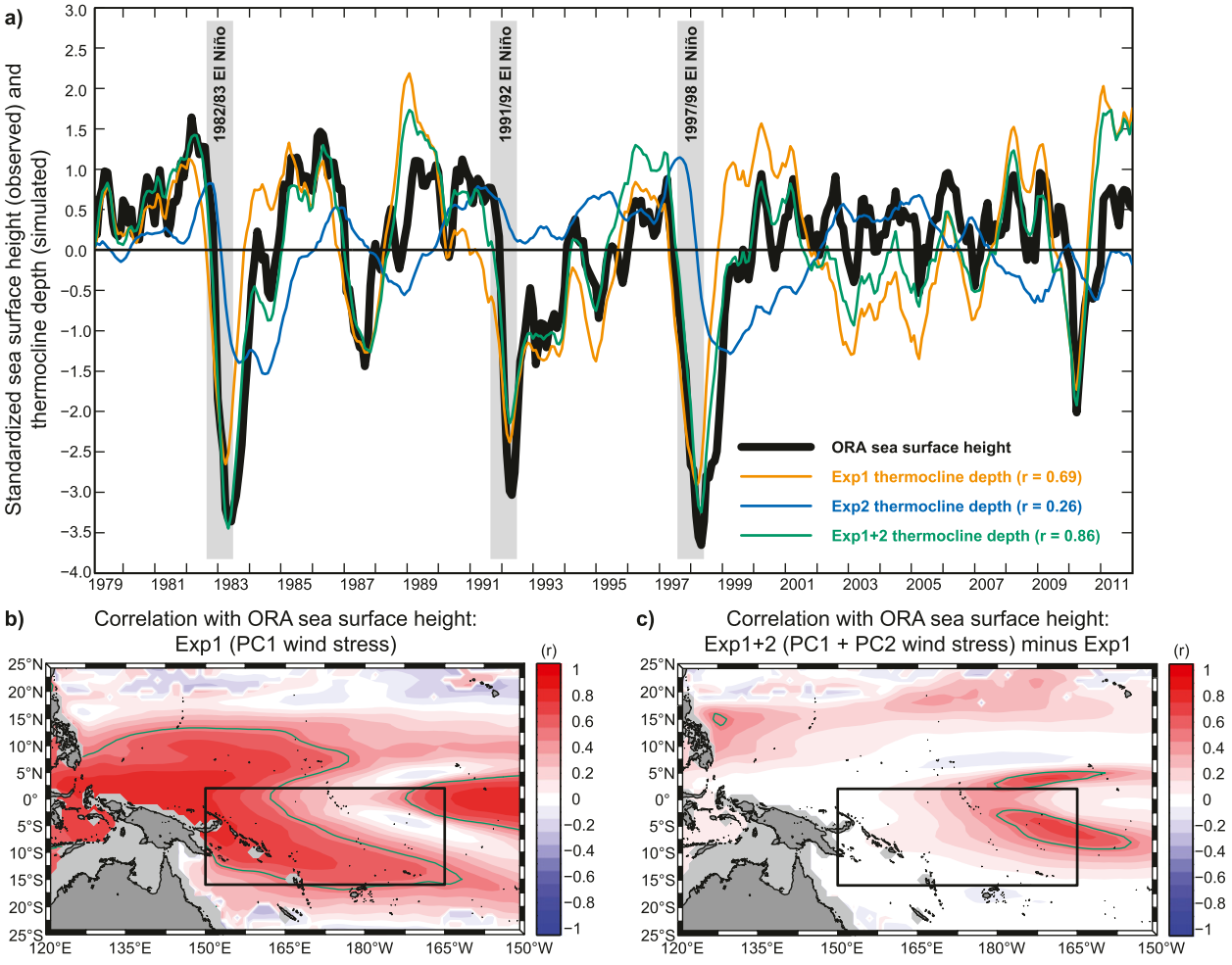

FIG. 7. (a) Standardized ORA sea surface height observations in the southwest Pacific (black) along with hindcast-simulated thermocline depths from SWM experiments forced with anomalous wind stresses reconstructed from either PC1 (orange, $r = 0.69$), PC2 (blue, $r = 0.26$), or PC1 + PC2 (green, $r = 0.86$) of the observations shown in Fig. 1. Simulated thermocline depths are divided by the standard deviation of the experiment forced with PC1 + PC2. Correlation coefficients between observations and respective simulations (green contours enclose $r > 0.5$): (b) PC1 wind stress and (c) PC1 + PC2 wind stresses minus PC1 wind stress. Black box indicates the southwest Pacific region (as defined in Fig. 1).

such as 1986/87 and 2009/10, by the occurrence of a zonal SPCZ and the associated meridional sea level response to wind stress anomalies.

Meridional asymmetry of the sea level response to ENSO is related to interaction of the tropical western Pacific annual cycle with interannual variations of SST-driven wind stress anomalies. As recently shown in Stuecker et al. (2013), spectral peaks of surface winds at frequencies $1 - f_E$ and $1 + f_E$ on either side of the annual frequency are near-annual combination tones that originate from a nonlinear interaction between ENSO and the annual cycle of SST forcing. During El Niño taimasa, seasonal development of the SPCZ in austral summer is a key element in generating the observed southward wind anomaly shift (McGregor et al. 2012b) and the corresponding wind stress curl anomalies that in turn cause the interhemispheric tropical sea level seesaw, mostly via oceanic Ekman pumping. Other, nonlocalized, processes such as planetary wave dynamics may explain some of the differences between sea surface height and wind stress curl seen in Figs. 1b,c, especially in the tropical northwestern Pacific where Rossby wave effects dominate (Chang et al. 2013).

Persistence of below-normal sea level in the southwest Pacific (Fig. 3) and the central Pacific (Figs. 4b,d) occurs most prominently after El Niño taimasa events (i.e., after extreme PC1 and PC2 wind stress peaks; see Fig. 1a). Recently, McGregor et al. (2013) related the nonlinear response of the South Pacific climate to ENSO and found that the role of PC2 wind stress is

Unauthenticated | Downloaded 04/28/25 08:15 PM UTC

greatest during the strongest El Niño events (extreme PC1 > 0). This is consistent with the idea that PC2 can be approximated as the product between the annual cycle and PC1, as shown in Stuecker et al. (2013). Conversely, during weaker El Niño events (including Modoki events) and also La Niña, there is a smaller SPCZ response and little southward propagation of wind stress anomalies. ENSO-dependent positioning of the SPCZ perhaps explains the asymmetric sea level response to El Niño taimasa, although a definitive association is limited by the small sample of zonal SPCZ events.

Given the well-established seasonal prediction skill for El Niño events and their seasonally paced termination, our analysis further suggests that long-duration extreme sea level drops in the equatorial central and tropical southwestern Pacific may also be highly predictable. Such predictability would provide advance warning to island communities who could perhaps act to adapt to the negative consequences of taimasa events, for instance, during coral die-offs. Further observational studies, along with more sophisticated hindcast experiments, are necessary to confirm the predictability of future El Niño taimasa impacts.

Finally, we caution that state-of-the-art coupled climate models forced with increasing greenhouse gas concentrations project a near doubling of the frequency of certain types of strong El Niño events during the twenty-first century (Cai et al. 2012)—events that shift the SPCZ equatorward, alter the trade winds locally, and that we have linked to taimasa. Should the future increased frequency of El Niño taimasa events verify, a higher likelihood of prolonged low sea level events is perceivable for the vulnerable islands in the tropical southwestern Pacific, even as this region continues to deal with global sea level rise associated with greenhouse gas related warming.

Acknowledgments. This study benefited from insightful discussions with Doug Fenner, Matt Kendall, Mark Merrifield, Doug Pirhalla, Bo Qui, and Roberto Venegas. We thank the National Marine Sanctuary of American Samoa for providing a unique cultural perspective of extreme low sea levels, locally called taimasa. This work was supported by NSF Grant 1049219 and by the International Pacific Research Center, which is funded jointly by the Japan Agency for Marine–Earth Science and Technology (JAMSTEC) and NOAA. We gratefully acknowledge additional support through sponsorship of research at IPRC by the Joint Institute for Marine and Atmospheric Research (JIMAR). SM was supported by the Australian Research Council. MFS was supported by NSF through Grant ATM1034798 and the U.S. Department of Energy through Grant DESC005110.

REFERENCES

Adler, R. F., and Coauthors, 2003: The version-2 Global Precipitation Climatology Project (GPCP) monthly precipitation analysis (1979–present). *J. Hydrometeor.,* **4,** 1147–1167.

Alory, G., and T. Delcroix, 2002: Interannual sea level changes and associated mass transports in the tropical Pacific from TOPEX/Poseidon data and linear model results (1964–1999). *J. Geophys. Res.,* **107,** 3153, doi:10.1029/2001JC001067.

Becker, M., B. Meyssignac, C. Letetrel, W. Llovel, A. Cazenave, and T. Delcroix, 2012: Sea level variations at tropical Pacific islands since 1950. *Global Planet. Change,* **80–81,** 85–98, doi:10.1016/j.gloplacha.2011.09.004.

Cai, W., and Coauthors, 2012: More extreme swings of the South Pacific convergence zone due to greenhouse warming. *Nature,* **488,** 365–369, doi:10.1038/nature11358.

Chang, Y.-T., L. Du, S.-W. Zhang, and P.-F. Huang, 2013: Sea level variations in the tropical Pacific Ocean during two types of recent El Niño events. *Global Planet. Change,* **108,** 119–127, doi:10.1016/j.gloplacha.2013.06.001.

Cheng, B., and E. Gaskin, 2011: Climate impacts to the nearshore marine environment and coastal communities: American Samoa and Fagatele Bay National Marine Sanctuary. Marine Sanctuaries Conservation Series ONMS-11-05, NOAA/Office of National Marine Sanctuaries, 71 pp.

Chowdhury, M. R., P. S. Chu, and T. Schroeder, 2006: ENSO and seasonal sea-level variability—A diagnostic discussion for the U.S.-Affiliated Pacific Islands. *Theor. Appl. Climatol.,* **88,** 213–224, doi:10.1007/s00704-006-0245-5.

Dee, D. P., and S. P. Uppala, 2009: Variational bias correction of satellite radiance data in the ERA-Interim reanalysis. *Quart. J. Roy. Meteor. Soc.,* **135,** 1830–1841.

Delcroix, T., 1998: Observed surface oceanic and atmospheric variability in the tropical Pacific at seasonal and ENSO timescales: A tentative overview. *J. Geophys. Res.,* **103** (C9), 18 611–18 633.

Harrison, D. E., and G. A. Vecchi, 1999: On the termination of El Niño. *Geophys. Res. Lett.,* **26,** 1593–1596.

Jin, F.-F., 1997: An equatorial ocean recharge paradigm for ENSO. Part I: Conceptual model. *J. Atmos. Sci.,* **54,** 811–829.

Kilarski S., and A. R. Everson, Eds., 2008: *Proceedings of the American Samoa Coral Reef Fishery Workshop*. NOAA Tech. Memo. NMFS-F/SPO114, 143 pp.

Leith, C. E., 1973: The standard error of time-averaged estimates of climatic means. *J. Appl. Meteor.,* **12,** 1066–1069.

McGregor, S., N. J. Holbrook, and S. B. Power, 2007: Interdecadal sea surface temperature variability in the equatorial Pacific Ocean. Part I: The role of off-equatorial wind stresses and oceanic Rossby waves. *J. Climate,* **20,** 2643–2658.

——, A. S. Gupta, and M. H. England, 2012a: Constraining wind stress products with sea surface height observations and implications for Pacific Ocean sea level trend attribution. *J. Climate,* **25,** 8164–8176.

——, A. Timmermann, N. Schneider, M. F. Stuecker, and M. H. England, 2012b: The effect of the South Pacific convergence zone on the termination of El Niño events and the meridional asymmetry of ENSO. *J. Climate,* **25,** 5566–5586.

——, N. Ramesh, P. Spence, M. H. England, M. J. McPhaden, and A. Santoso, 2013: Meridional movement of wind anomalies

Unauthenticated | Downloaded 04/28/25 08:15 PM UTC

during ENSO events and their role in event termination. *Geophys. Res. Lett.,* **40,** 749–754, doi:10.1002/grl.50136.

Meinen, C. S., and M. J. McPhaden, 2000: Observations of warm water volume changes in the equatorial Pacific and their relationship to El Niño and La Niña. *J. Climate,* **13,** 3551–3559.

Merrifield, M. A., and M. E. Maltrud, 2011: Regional sea level trends due to a Pacific trade wind intensification. *Geophys. Res. Lett.,* **38,** L21605, doi:10.1029/2011gl049576.

——, B. Kilonsky, and S. Nakahara, 1999: Interannual sea level changes in the tropical Pacific associated with ENSO. *Geophys. Res. Lett.,* **26,** 3317–3320, doi:10.1029/1999gl010485.

——, P. R. Thompson, and M. Lander, 2012: Multidecadal sea level anomalies and trends in the western tropical Pacific. *Geophys. Res. Lett.,* **39,** L13602, doi:10.1029/2012gl052032.

Mogensen, K., M. A. Balmaseda, and A. Weaver, 2012: The NEMOVAR ocean data assimilation system as implemented in the ECMWF ocean analysis for system 4. ECMWF Tech. Memo. 668, 59 pp.

Nidheesh, A. G., M. Lengaigne, J. Vialard, A. S. Unnikrishnan, and H. Dayan, 2013: Decadal and long-term sea level variability in the tropical Indo-Pacific Ocean. *Climate Dyn.,* **41,** 381–402, doi:10.1007/s00382-012-1463-4.

Pirhalla, D., V. Ransi, M. S. Kendall, and D. Fenner, 2011: Oceanography of the Samoan Archipelago. A Biogeographic Assessment of the Samoan Archipelago, NOAA Tech. Memo. NOS NCCOS, 229 pp.

Qiu, B., and S. Chen, 2010: Interannual-to-decadal variability in the bifurcation of the North Equatorial Current off the Phillippines. *J. Phys. Oceanogr.,* **40,** 2525–2538.

Rebert, J. P., J. R. Donguy, G. Eldin, and K. Wyrtki, 1985: Relations between sea level, thermocline depth, heat content, and dynamic height in the tropical Pacific Ocean. *J. Geophys. Res.,* **90** (C6), 11 719–11 725.

Stuecker, M. F., A. Timmermann, F.-F. Jin, S. McGregor, and H.-L. Ren, 2013: A combination mode of the annual cycle and the El Niño/Southern Oscillation. *Nat. Geosci.,* **6,** 540–544, doi:10.1038/ngeo1826.

Thomson, D. J., 1982: Spectrum estimation and harmonic analysis. *Proc. IEEE,* **70,** 1055–1096.

Timmermann, A., S. McGregor, and F. F. Jin, 2010: Wind effects on past and future regional sea level trends in the southern Indo-Pacific. *J. Climate,* **23,** 4429–4437.

Vecchi, G. A., and D. E. Harrison, 2003: On the termination of the 2002-03 El Niño. *Geophys. Res. Lett.,* **30,** 1964, doi:10.1029/2003GL017564.

——, and ——, 2006: The termination of the 1997–98 El Niño. Part I: Mechanisms of oceanic change. *J. Climate,* **19,** 2633–2646.

Vincent, D. G., 1994: The South Pacific convergence zone (SPCZ): A review. *Mon. Wea. Rev.,* **122,** 1949–1970.

Vincent, E. M., M. Lengaigne, C. E. Menkes, N. C. Jourdain, P. Marchesiello, and G. Madec, 2011: Interannual variability of the South Pacific convergence zone and implications for tropical cyclone genesis. *Climate Dyn.,* **36,** 1881–1896, doi:10.1007/s00382-009-0716-3.

Wang, B., R. Wu, and R. Lukas, 1999: Roles of the western North Pacific wind variation in thermocline adjustment and ENSO phase transition. *J. Meteor. Soc. Japan,* **77,** 1–16.

Widlansky, M. J., P. J. Webster, and C. D. Hoyos, 2011: On the location and orientation of the South Pacific convergence zone. *Climate Dyn.,* **36,** 561–578, doi:10.1007/s00382-010-0871-6.

——, A. Timmermann, K. Stein, S. McGregor, N. Schneider, M. H. England, M. Lengaigne, and W. Cai, 2013: Changes in South Pacific rainfall bands in a warming climate. *Nat. Climate Change,* **3,** 417–423, doi:10.1038/nclimate1726.

Woodroffe, C. D., M. R. Beech, and M. K. Gagan, 2003: Mid-late Holocene El Niño variability in the equatorial Pacific from coral microatolls. *Geophys. Res. Lett.,* **30,** 1358, doi:10.1029/2002GL015868.

Wyrtki, K., 1984: The slope of sea level along the equator during the 1982/1983 El Niño. *J. Geophys. Res.,* **89** (C6), 10 419–10 424.

——, 1989: Some thoughts about the west Pacific warm pool. *Western Pacific Int. Meeting and Workshop on TOGA COARE,* Nouméa, New Caledonia, Institut Français de Recherche Scientifique pour le Développement en Coopération, 99–109.

Zhang, X., and J. A. Church, 2012: Sea level trends, interannual and decadal variability in the Pacific Ocean. *Geophys. Res. Lett.,* **39,** L21701, doi:10.1029/2012GL053240.

Unauthenticated | Downloaded 04/28/25 08:15 PM UTC